Synthesis and Characteristics of Al-containing ZSM-58 Zeolite Membrane for CO_2 Separation

E. Hayakawa and S. Himeno

***Abstract*—We prepared an Al-containing ZSM-58 zeolite membrane and compared it with the separation performance of an all-silica ZSM-58 zeolite membrane. First, the ZSM-58 zeolite crystals were synthesized from a solution with the same membrane synthesis solution composition, and the characteristics of ZSM-58 zeolite crystals with a difference in Si/Al molar ratio were studied. As-made crystals should have high porosity and crystallinity. All-silica and Al-containing ZSM-58 zeolite membranes were applied in the separation of an equimolar CO_2/CH_4 and CO_2/N_2 mixture of pressure drop and temperature. The Al-containing ZSM-58 zeolite membrane showed a higher selectivity than the all-silica ZSM-58 zeolite membrane, which was confirmed at a lower temperature and feed pressure.**

***Index Terms*—CO_2 separation, DDR type zeolite, zeolite membrane, ZSM-58.**

I. Introduction

Carbon dioxide is a cause of global warming, and CO_2 recovery technology for natural and flue gases is important in this regard. Among other separation technologies, a membrane separation method for CO_2 recovery can achieve higher energy and space savings and better economic characteristics. In particular, because the zeolite with an eight-membered oxygen ring (DDR, CHA, AEI, etc.) has pores close in molecular size to CO_2, N_2, and CH_4 [1]–[14], it is a promising material for a CO_2 separation membrane.

DD3R zeolite has an all-silica DDR topology and has pores (0.36 × 0.44 nm) with an intermediate size between those of CO_2 molecules (0.33 nm) and CH_4 molecules (0.38 nm) [15]. Thus, many researchers have studied DD3R zeolite as a CO_2 separation membrane and reported a high CO_2/CH_4 separation performance [1], [4], [6], [16], [17]. By contrast, ZSM-58 zeolite has a DDR topology of Al-containing zeolite, which was reported to have a Si/Al molar ratio of 20 to ∞ [18]. Al-containing zeolite has certain functions such as an ion exchange capacity and solid acid point.

Al-containing zeolite also has an increased CO_2 adsorption capability according to the decrease in Si/Al ratio [19], [20].

For example, adsorption CO_2/CH_4 selectivity of the LTA zeolite increased approximately 15 times if the Si/Al ratio of the LTA zeolite changed from ∞ to 2. Al-containing zeolite can be applied to pore size control using an ion exchange capacity such as from Na, K, Pb, and Pt [21], [22]. In addition, amine-modified zeolite has a high affinity for CO_2 [23].

Therefore, an Al-containing ZSM-58 zeolite membrane is expected to have a higher CO_2/CH_4 and CO_2/N_2 separation selectivity than DD3R, and an ion exchange and surface modification technology can be applied. However, it is difficult to prepare Al-containing zeolite membrane with high gas separation performance due to electrostatic repulsive force between silicate anion and negatively charged Al atom in zeolite framework [24], [25]. The synthesis of an all-silica ZSM-58 zeolite membrane was reported by Choi *et al.* [26]. However, there has been no reported synthesis of an Al-containing ZSM-58 zeolite membrane. In this study, we prepared an Al-containing ZSM-58 zeolite membrane, and investigated the separation characteristics of CO_2/CH_4 and CO_2/N_2 through a comparison with an all-silica ZSM-58 zeolite membrane.

Manuscript received August 25, 2019; revised October 31, 2019.

Eiji Hayakawa and Shuji Himeno are with the Department of Science of Technology Innovation, Nagaoka University of Technology, 1603-1, Kamitomioka-cho, Nagaoka, Niigata 940-2188, Japan (e-mail: e_hayakawa@stn.nagaokaut.ac.jp, himeno@vos.nagaokaut.ac.jp).

II. Experimental

A. Materials and Chemicals

The following chemicals and materials were used in the resent work: Ludox HS-30 colloidal silica (30 wt%, Sigma-Aldrich), sodium hydroxide (97.0%, Wako), potassium hydroxide (85%, Wako), sodium aluminate (Al/NaOH molar ratio = 0.77, Wako), tropine (98%, Combi-Blocks), iodomethane (99.5%, Wako), and ethanol (95%, Wako). In addition, CO_2 (99%), CH_4 (99%), and N_2 (99%) were used for the gas permeation tests.

TABLE I: Properties of Porous a-Alumina Tubular Support

Outer diameter (mm)	Length (mm)	Porosity (%)	Pore diameter (μm)		
			Surface	Middle	Support
10	100	30-50	0.2	0.9	2-3

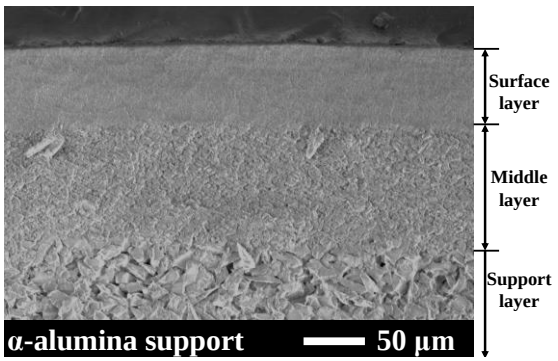

Fig. 1. Cross-sectional SEM image of α-alumina tubular support used in this study.

The ZSM-58 zeolite membranes were prepared on the outside surface of porous α-alumina tubes (NGK Insulators, Ltd.). The porous α-alumina tubular supports used in this study are summarized in Table I. Fig. 1 shows a cross-section of scanning electron microscopy (SEM) image of a porous

doi: 10.18178/ijcea.2020.11.1.771

α-alumina tubular support. This support consists of three layers, namely, the surface, middle, and support layers. Moreover, the pore diameter of the surface layer is 0.2 μm, and the length of the support is 30 or 100 mm. This support has a CO_2 permeance of 4×10^{-5} mol/s/m^2/Pa at a feed pressure of 0.1 MPa. The CO_2 permeance of the DDR zeolite membrane is from 10^{-8} to 10^{-7} mol/s/m^2/Pa, and the porous support has a sufficiently higher permeance than the zeolite layer.

B. Prepared ZSM-58 Seed Crystals and Seed Slurry

We prepared a ZSM-58 seed crystal by referencing a report by Valyocsik *et al*. [27]. Methyltropinium iodide (MTI) was used for the synthesis of the ZSM-58 zeolite as the structure directing agent (SDA). For the synthesis of MTI, 25.0 g of tropine was first dissolved in 100 g of ethanol. Next, 25.1 g of methyl iodide was then added to the solution, and the suspension was maintained under a reflux for 72 h. After cooling, the as-made MTI was washed with ethanol and dried at 343 K.

For the synthesis of the ZSM-58 crystals, a precursor solution with a composition molar ratio of MTI : NaOH : SiO_2 : H_2O = 0.25 : 0.33 : 1 : 40 was used. The precursor solution was prepared as follows: 6.4 g MTI was added to 42.9 g of H_2O (solution A), and 9.97 ml of a 3 M NaOH solution and 18.2 g of Ludox HS-30 were then added to solution A and stirred for 24 h (solution B). Solution B was then transferred into a Teflon-lined autoclave and maintained at 433 K for 72 h under rotation stirring. The as-synthesized ZSM-58 zeolite seed crystals were washed with DI water. After drying at 343 K overnight, ZSM-58 seed crystals were calcined at 973 K for 4 h at a ramp rate of 0.5 L min^{-1}. The calcined ZSM-58 zeolite particles were then milled, and the ball-milled particles were then dispersed in DI water, and ZSM-58 seed slurry with a particle size distribution of 0.2 μm was prepared using a centrifugation method. The ball-milled ZSM-58 seed particulates were coated onto the outermost surface layer of the alumina tubular support through a dip-coating method using this slurry. Fig. 2 shows an SEM image and X-ray diffraction (XRD) pattern of the ZSM-58 seed crystals in this work.

C. Synthesis of ZSM-58 Zeolite Crystals

We used the preparation method of a precursor solution as reported by Kumita *et al*. [28]. First, KOH and Ludox HS-30 were added to deionized water, and the solution was stirred for 20 min (solution A). The MTI, KOH, and deionized water were mixed in another container (solution B). If the Al-containing ZSM-58 zeolite was prepared, sodium aluminate was added into solution B. Solutions A and B were mixed and stirred for 24 h at 313 K. The samples of c1 and c2 had molar compositions of 0.1MTI : 0.1KOH : 1SiO_2 : 52H_2O and 0.05MTI : 0.05KOH : 1SiO_2 : 0.014Al_2O_3 : 52H_2O, respectively.

Next, 0.01 wt% of the ZSM-58 seed crystals were added to the precursor solution, and hydrothermal treatment was conducted at 413 K. The holding time of the hydrothermal treatment was two (c1) or five (c2) days. After hydrothermal treatment, the as-made crystals were washed with ethanol and deionized water and dried overnight at 343 K. The ZSM-58 zeolite crystals were calcined at 823 K for 4 h at a ramp rate of 0.5 L min^{-1}.

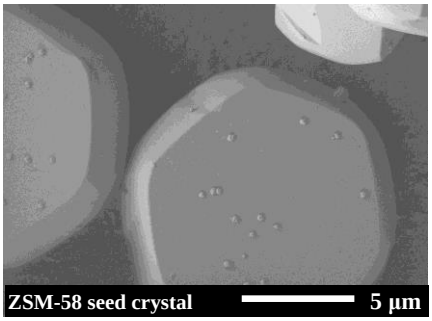

(a)

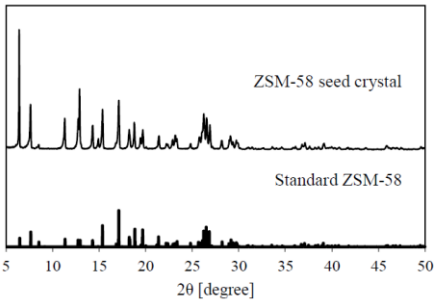

(b)

Fig. 2. (a) SEM image, (b) XRD pattern of ZSM-58 zeolite seed crystals.

D. Synthesis of ZSM-58 Zeolite Membrane with Difference in Si/Al Molar Ratio

Ball-milled ZSM-58 seed particulates were coated onto the outermost surface layer of the alumina tubular support using a dip-coating method with ZSM-58 seed slurry. The ZSM-58 zeolite membranes were synthesized through a secondary growth method on the surface layer of the porous α-alumina tubular support. The precursor solution was prepared using a ZSM-58 zeolite crystal method (refer to Section 2.3), and all-silica (M1) and Al-containing ZSM-58 (M2) membranes were prepared using a gel composition of c1 and c2, respectively.

A α-alumina tubular support coated ZSM-58 seed crystal was placed vertically in a Teflon liner autoclave. A synthesis gel was then transferred into the Teflon liner autoclave and hydrothermal treatment was conducted at 413 K for two (M1) or five (M2) days. The autoclave was then cooled to room temperature, and the as-made membrane was washed with boiling water and dried at 343 K overnight. Different calcination methods were applied to M1 and M2 to inhibit the generation of cracks in the zeolite membrane.

An ozone de-template method was applied to M1 [16, 29], which was calcined at 473 K for 24 h under an ozone concentration of 120 g/Nm^3 at a flow rate of 1 L/min.

A rapid thermal process (RTP) and a thermal calcination method were applied to M2 (Al-containing membrane) [17, 30]. M2 was then directly loaded into a preheated muffle furnace at 973 K for 1 min, withdrawn quickly, and cooled to room temperature. The ZSM-58 zeolite membrane was then calcined at 823 K for 4 h at a ramp rate of 0.5 L min^{-1}.

E. Characterization of ZSM-58 Zeolite Crystals and Membrane

The XRD (XRD-6100, Shimadzu) patterns were recorded using Cu Kα radiation. SEM images were obtained using a field-emission scanning electron microscope (JSM-6701, JEOL Ltd.) under an accelerating voltage of 1 kV and a work

distance of 8–11 mm. The N_2 adsorption isotherms were measured using a BELSORP-Max (MicrotracBEL Co.) at 77 K. An elemental analysis of the ZSM-58 zeolite crystals was conducted using X-ray fluorescence (XRF, Rigaku ZSX Primus II, Rigaku Co.) analysis.

F. Gas Permeation and Separation Measurement

Single- and mixture-gas permeance tests using CO_2, CH_4, and N_2 were carried out on the ZSM-58 zeolite membranes. In this study, an equimolar mixture gas (CO_2/CH_4 and CO_2/N_2) was used to evaluate the permeance characteristics of the ZSM-58 zeolite membranes.

Single- and equimolar-mixture permeance tests as a function of the total feed pressure or temperature were also carried out on the ZSM-58 zeolite membranes. The total feed pressure was 0.3–0.9 MPa, and the permeate pressure was approximately 0.1013 MPa (atmospheric pressure). The gas permeation temperature was maintained at 273, 298, 348, 398, or 448 K. The gas flux and concentration were determined using a soap film flowmeter and gas chromatograph, respectively (490 Micro GC, GL Science).

The permeance, P_i (mol/s/m^2/Pa), was calculated using the following formula:

$$P_i = \frac{Q_i}{A \cdot t \cdot \Delta p_i}$$

where Q_i (mol) is the mole of component i permeated through the membrane for a time of t (s), A (m^2) is the membrane area, and Δp_i (Pa) is the differential partial pressure of component i between the feed and permeate side.

The ideal selectivity is the ratio of the single-gas permeance. The separation selectivity is the ratio of the mixture-gas permeance. Therefore, the separation selectivity (P_i/P_j) for components i over j was calculated using the following formula:

$$\text{Selectivity} = \frac{P_i}{P_j}$$

Then, error rate of CO_2 permeance and CH_4 or N_2 permeance was approximately ± 0.6 and $\pm 7\%$, respectively. Moreover, the error rate of selectivity was approximately $\pm$ 7%. The error rates were calculated from the standard deviation of the gas permeation time (t) and gas concentration.

III. Results and Discussion

A. Research into Properties from N_2 Adsorption Isotherm of ZSM-58 Zeolite Crystals with Difference in Si/Al Molar Ratio

First, we investigated a N_2 adsorption isotherm of ZSM-58 zeolite crystal with a difference in Si/Al molar ratio. Here, c1 and c2 were prepared using a precursor solution with a Si/Al molar ratio of ∞ and 70, respectively. Based on XRF, c2 was confirmed to have a Si/Al molar ratio of 81 in the crystals. Figs. 3 and 4 show an SEM image and XRD pattern of c1 and c2, respectively. The as-made crystals had a rhombohedral shape, which was confirmed using a DD3R crystal reported in a previous study, and confirmed a high crystallinity through the XRD pattern.

Figs. 5 and 6 respectively show N_2 adsorption isotherm and the FT-IR spectrum of as-made ZSM-58 zeolite crystals. Table II shows the characteristics of the ZSM-58 zeolite crystals based on the measured N_2 adsorption isotherm.

The as-made crystals had a type I adsorption isotherm, which is obtained in microporous materials [31]. The ZSM-58 zeolite showed a BET surface area of from 300 to 400 m^2/g, which is consistent with the previous reports.

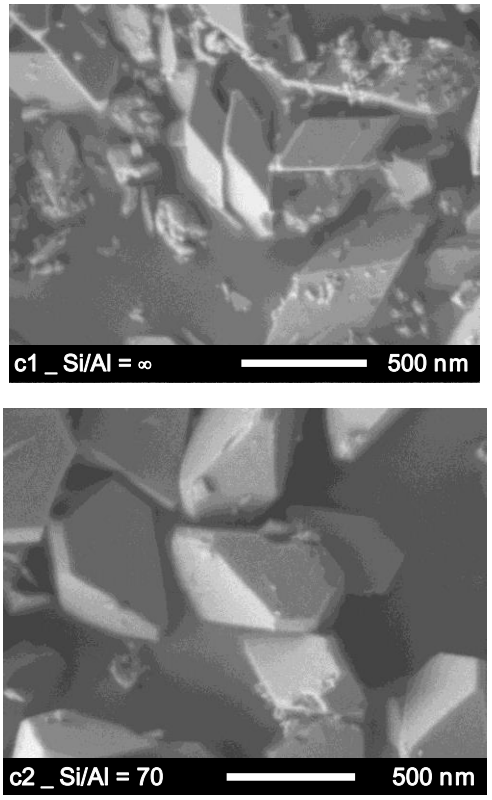

Fig. 3. SEM images of c1 of Si/Al = ∞ and c2 of Si/Al = 70.

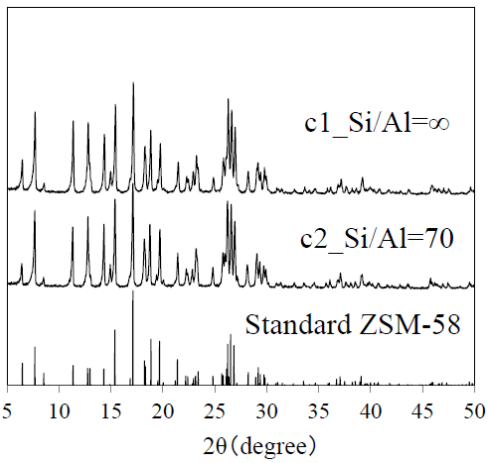

Fig. 4. XRD patterns of c1 of Si/Al = ∞ and c2 of Si/Al = 70.

TABLE II: N_2 Adsorption Characterization of ZSM-58 Zeolite Crystals with Difference in Si/Al Molar Ratio

No.	Si/Al	BET Surface Area (m^2/g)	Micropore volume (cm^3/g)	Total pore volume (cm^3/g)
c1	∞	388	0.16	0.24
c2	70	355	0.13	0.23

In addition, c1 (Si/Al = ∞) showed a higher BET surface area than c2 (Si/Al = 70), and a similar tendency for BET

surface area was reported by Kuhn *et al.* [32] because the template removal is difficult for zeolites with a low Si/Al ratio [33].

Meanwhile, FT-IR spectrums of zeolite crystals showed conformed peaks of C-H bonds of MTI molecules assigned from 2,800 to 3,000 and from 1,400 to 1,500 cm^{-1}. Therefore, MTI molecules in ZSM-58 zeolite pores were able to be removed through thermal calcination at 823 K.

B. Characterization of ZSM-58 Zeolite Membrane

Fig. 7 shows XRD pattern of a ZSM-58 membrane, which suggests that M1 and M2 have a high purity ZSM-58 zeolite layer. As shown in Figs. 8 and 9, M1 is covered with approximately 1 μm of ZSM-58 polycrystalline grains, and the membrane thickness, including the composition layer, is approximately 5 μm. In contrast, M2 showed a larger polycrystalline grain and thicker membrane thickness than M1.

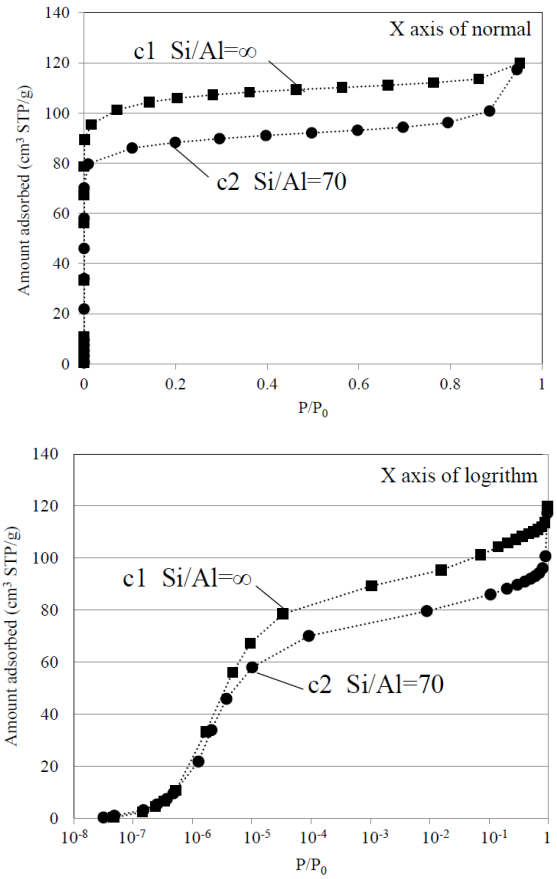

Fig. 5. Normal x and logarithmic x of N_2 adsorption isotherm (at 77 K) of ZSM-58 zeolite crystals of c1 of Si/Al = ∞ and c2 of Si/Al = 70.

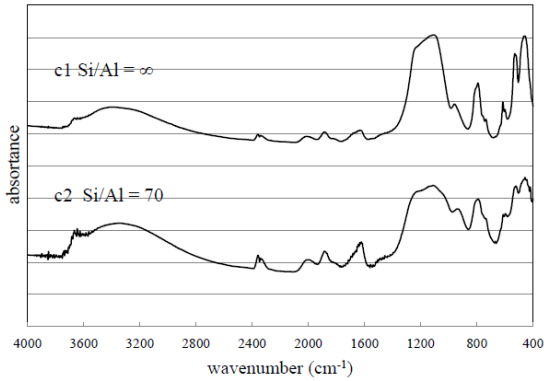

Fig. 6. FT-IR spectrum of c1 of Si/Al = ∞ and c2 of Si/Al = 70.

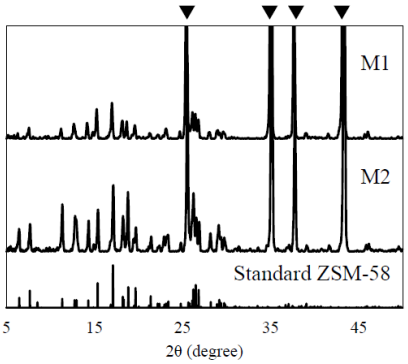

Fig. 7. XRD patterns of M1 and M2. The triangles (▼) indicate the α-alumina peak.

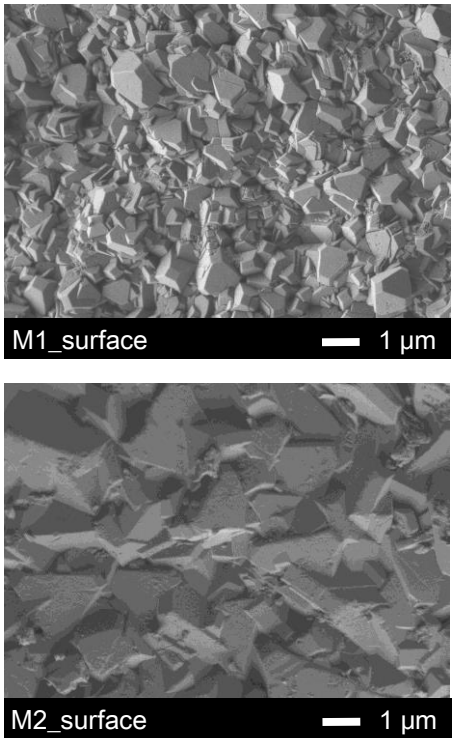

Fig. 8. SEM images of membrane surface of M1 and M2.

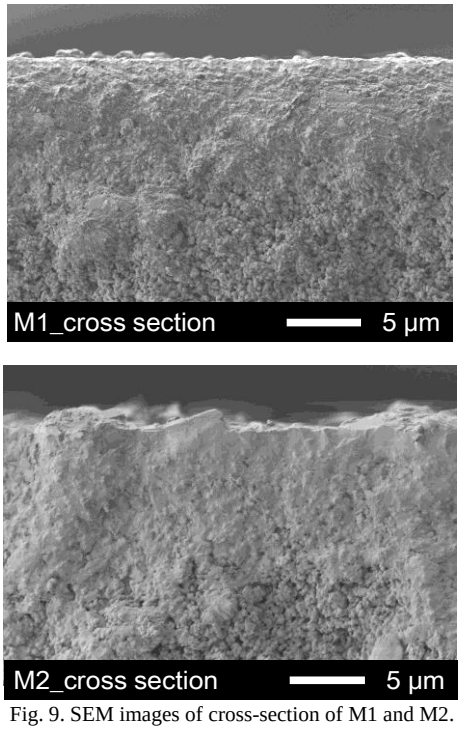

Fig. 9. SEM images of cross-section of M1 and M2.

C. Effect of Pressure Drop at CO_2/CH_4 Condition

Fig. 10 shows the pressure dependence of single and mixture permeance (single P_{CO2} and P_{CH4}, and mixed P_{CO2} and P_{CH4}) through all-silica (M1) and Al-containing ZSM-58 zeolite membranes (M2). M1 showed a mixed P_{CO2} of 17 × 10^{-8} mol/s/m^2/Pa and single P_{CO2} of 26 × 10^{-8} mol/s/m^2/Pa, whereas M2 had a P_{CO2} mixture of 6.3 × 10^{-8} mol/s/m^2/Pa and single P_{CO2} of 9.1 × 10^{-8} mol/s/m^2/Pa at a pressure decrease of 0.2 MPa. Because M2 has a dense and thick zeolite layer, it shows a P_{CO2} of approximately 40% of M1.

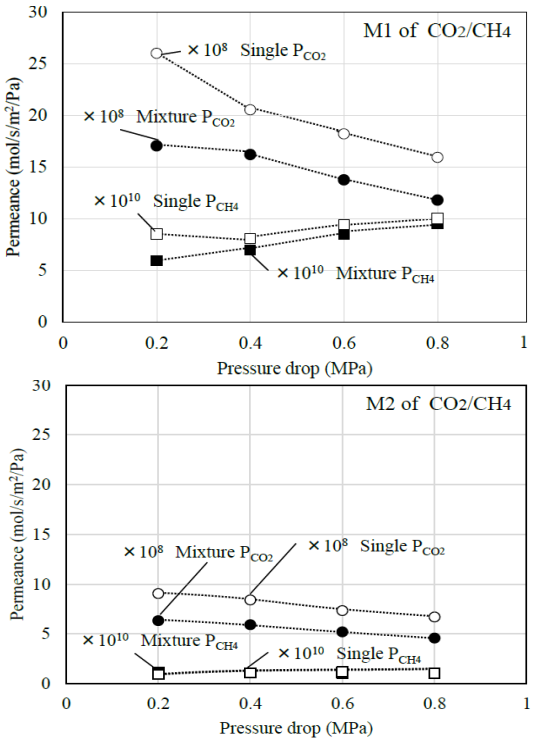

Fig. 10. Permeance of single-gas and equimolar CO_2/CH_4 mixture with pressure drop at 298 K, and permeated side of atmospheric pressure for M1 and M2. Open symbols (○, □) indicate the single-gas permeance of CO_2 and CH_4, and closed symbols (●, ■) indicate the mixture permeance of CO_2 and CH_4.

The single and mixed P_{CO2} decreased with an increase in pressure drop because the adsorption of CO_2 molecules in the zeolite pores became saturated at a high-pressure region.

The value of P_{CH4} for M1 increased as the pressure drop increased, whereas that for M2 was independent of the pressure drop. This difference is speculated to be due to the amount of large crystal grains.

The M2 was calcined through RTP and the thermal calcination method. It is thought that the rapid thermal treatment caused a bonding surface silanol of the zeolite crystal and inhibited the cracks and large crystal grains [17]. However, because there is no effect of RTP treatment owing to few surface silanol groups in the all-silica zeolite membrane, ozone de-template method was applied to M2. As a result, M2 shows an extremely low P_{CH4}, and a very high P_{CO2}/P_{CH4}, as shown in Fig. 11.

D. Effects of Temperature at CO_2/CH_4 Condition

Fig. 12 and 13 shows the pressure dependence of single gas and mixture permeance and CO_2/CH_4 selectivity through M1 and M2. M1 showed a P_{CO2} mixture of 21 × 10^{-8} mol/s/m^2/Pa and single P_{CO2} of 31 × 10^{-8} mol/s/m^2/Pa, whereas M2 showed a P_{CO2} mixture of 14 × 10^{-8} mol/s/m^2/Pa and single P_{CO2} of 16 × 10^{-8} mol/s/m^2/Pa at a temperature of 273 K.

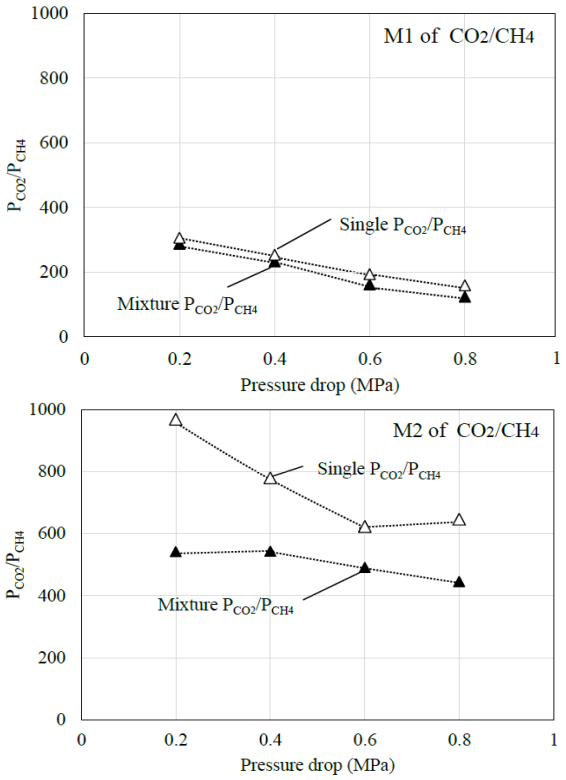

Fig. 11. P_{CO2}/P_{CH4} of single-gas and equimolar CO_2/CH_4 mixture of pressure drop at 298 K, and permeated side of atmospheric pressure for M1 and M2. Open symbols (△) correspond to single-gas selectivity of CO_2 and CH_4, and closed symbols (▲) correspond to the mixture permeance of CO_2 and CH_4.

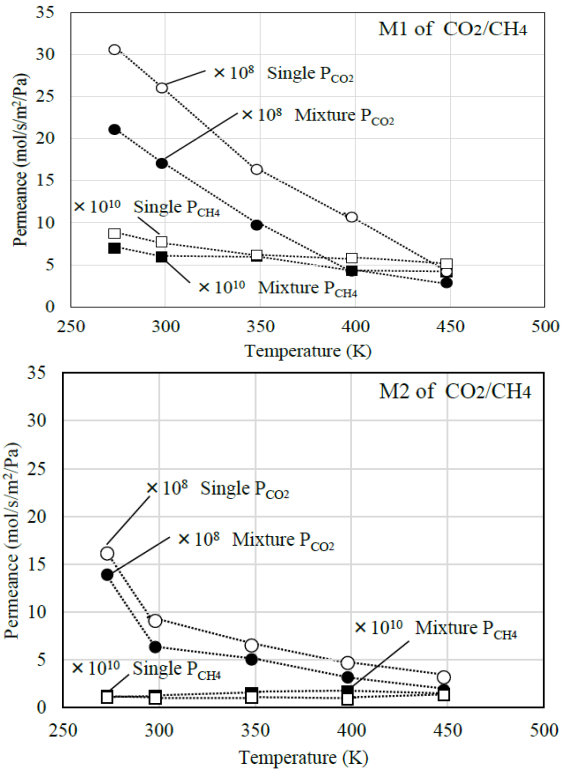

Fig. 12. Permeance of single gas and equimolar CO_2/CH_4 mixture with temperature at a pressure drop of 0.2 MPa and permeated side of atmospheric pressure for M1 and M2. Open symbols (○, □) correspond to the single-gas permeance of CO_2 and CH_4, and closed symbols (●, ■) correspond to the mixed permeance of CO_2 and CH_4.

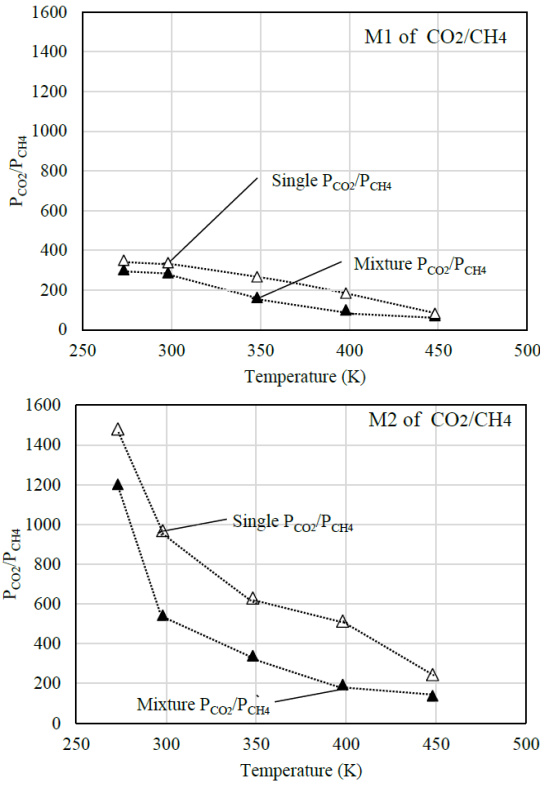

Fig. 13. P_{CO2}/P_{CH4} of single gas and equimolar CO_2/CH_4 mixture as a function of temperature at a pressure drop of 0.2 MPa and permeated side of atmospheric pressure for M1 and M2. Open symbols (△) correspond to the single-gas selectivity of CO_2 and CH_4, and the closed symbols (▲) correspond to the mixture permeance of CO_2 and CH_4.

Because the CO_2 adsorption coverage decreased as the temperature increased, the single and mixed P_{CO2} decreased according to the increased separation temperature. The P_{CO2} and P_{CO2}/P_{CH4} of M2 were significantly high at 273 K. Al-containing zeolite strongly adsorbs CO_2 molecules in low temperature. Therefore, M2 (single, 1,500; mixed, 1,200) has a higher P_{CO2}/P_{CH4} (single, 350; mixture, 300) than M1 at 273 K. In contrast, P_{CO2}/P_{CH4} of M2 (single, 240; mixture, 140) is close to P_{CO2}/P_{CH4} of M1 (single, 81; mixture, 71) at 448 K because the CO_2 adsorption coverage is low in a high-temperature region.

E. Effects of Pressure Drop at CO_2/N_2 Condition

Figs. 14 and 15 show the pressure dependence of the permeance (single P_{CO2} and P_{N2}, mixed P_{CO2} and P_{N2}) and CO_2/N_2 selectivity (single P_{CO2}/P_{N2}, and mixed P_{CO2}/P_{N2}) through M1 and M2, respectively. M1 showed a P_{CO2} mixture of 28 $\times 10^{-8}$ mol/s/m^2/Pa and P_{CO2}/P_{N2} mixture of 44, whereas M2 showed a P_{CO2} mixture of 12 $\times 10^{-8}$ mol/s/m^2/Pa and P_{CO2}/P_{N2} mixture of 53 of at a pressure drop of 0.2 MPa. As with the CO_2/CH_4 separation, P_{CO2} decreased as the pressure drop increased.

The single and mixed P_{N2} were independent of the pressure drop, and the mixed P_{N2} was higher than the single P_{N2} for both membranes. Here, P_{N2} was over 10-times that of P_{CH4}, which suggests that N_2 molecules diffused faster into zeolite pores than CH_4 molecules. Therefore, the CO_2/N_2 adsorption selectivity was important for CO_2/N_2 separation. N_2 permeation was inhibited owing to strongly adsorbed CO_2 molecules in the zeolite pore in the mixed system [16], [17].

The single P_{CO2}/P_{N2} of both membranes was in the range of 18–30, and a large difference was not confirmed. When the pressure drop was changed from 0.2 to 0.8 MPa, the mixture P_{CO2}/P_{N2} of M1 and M2 decreased from 44 to 30 and 53 to 45, respectively. Because zeolite with a low Si/Al molar ratio has a high CO_2 adsorption capacity [19], [20], we considered that M2 showed a higher P_{CO2}/P_{N2} than M1.

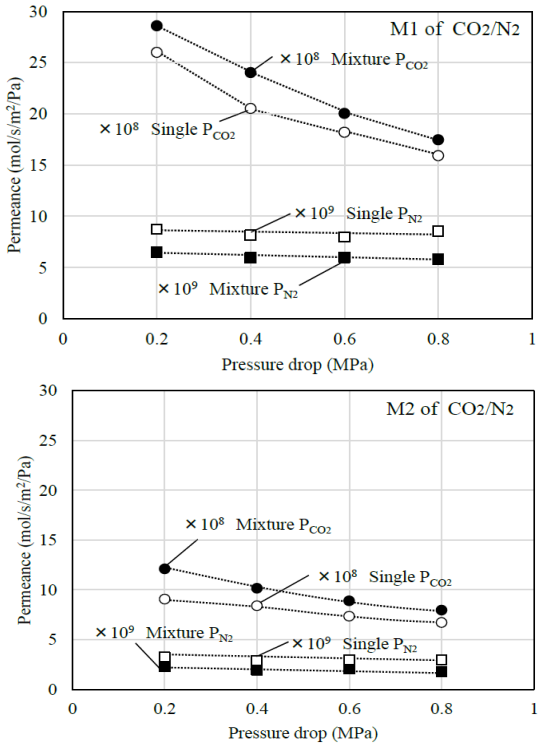

Fig. 14. Permeance of single-gas and equimolar CO_2/N_2 mixture of pressure drop at 298 K and permeated side of atmospheric pressure for M1 and M2. Open symbols (○, □) correspond to the single-gas permeance of CO_2 and N_2, and closed symbols (●, ■) correspond to the mixed permeance of CO_2 and N_2.

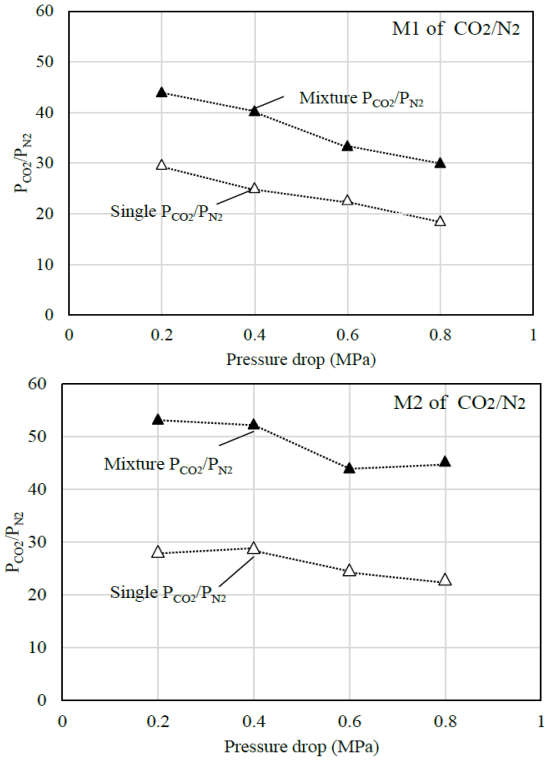

Fig. 15. P_{CO2}/P_{CH4} of single-gas and equimolar CO_2/N_2 mixture of pressure drop at 298 K and permeated side of atmospheric pressure for M1 and M2. Open symbols (△) correspond to the single-gas selectivity of CO_2 and N_2, and closed symbols (▲) correspond to the mixed permeance of CO_2 and N_2.

F. Effects of Temperature at CO_2/N_2 Condition

Figs. 16 and 17 show the temperature dependence of permeance and CO_2/N_2 selectivity through M1 and M2, respectively. M1 showed a P_{CO2} mixture of 34 × 10^{-8} mol/s/m^2/Pa and P_{CO2}/P_{N2} mixture of 57, whereas M2 showed P_{CO2} mixture of 17 ×10^{-8} mol/s/m^2/Pa and P_{CO2}/P_{N2} mixture of 64 at a temperature of 273 K.

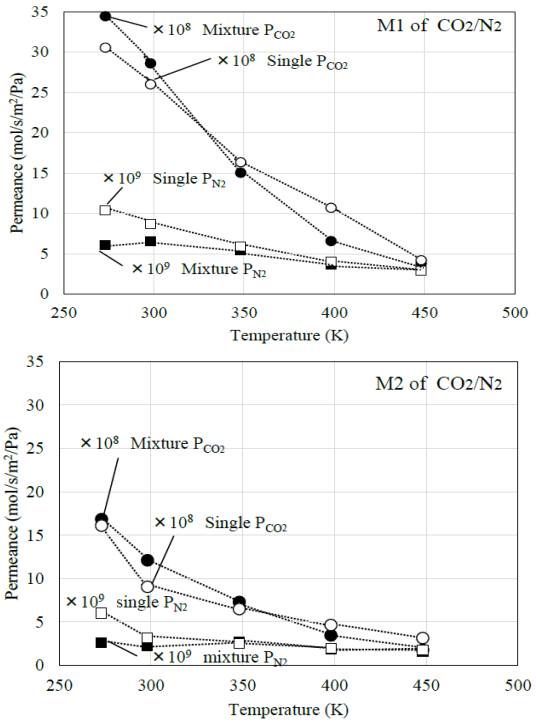

Fig. 16. Permeance of single-gas and equimolar CO_2/N_2 mixture as a function of temperature at a pressure drop of 0.2 MPa and permeated side of atmospheric pressure for M1 and M2. Open symbols (○, □) correspond to the single-gas permeance of CO_2 and N_2, and closed symbols (●, ■) correspond to the mixed permeance of CO_2 and N_2.

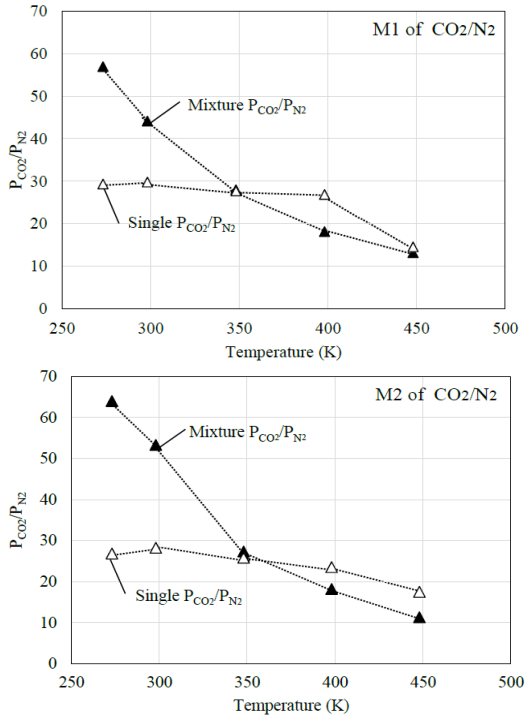

Fig. 17. $P_{CO2}//P_{N2}$ of single gas and equimolar CO_2/N_2 mixture as a function of temperature at a pressure drop of 0.2 MPa and the permeated side of atmospheric pressure for (a) M1 and (b) M2. Open symbols (△) correspond to the single gas selectivity of CO_2 and N_2, and closed symbols (▲) correspond to a mixed permeance of CO_2 and N_2.

Here, P_{CO2} and P_{N2} decreased as the temperature increased because the adsorption coverage decreased at a high temperature. Although the P_{CO2} and P_{CO2}/P_{N2} mixture was higher than a single system at less than 350 K, the magnitude of the correlation of P_{CO2} and P_{CO2}/P_{N2} between the mixed and single gases was reversed at over 350 K. Moreover, mixture P_{N2} was similar than single system at over 350 K. Their trend was caused by a suppression of the N_2 permeation owing to a high CO_2 adsorption coverage at low temperature (< 350 K).

However, CO_2 permeation was inhibited the adsorption competition between N_2 and CO_2 owing to the decrease in CO_2 adsorption coverage at high temperature, and the mixed P_{CO2} was lower than the single P_{CO2}. Therefore, P_{CO2} and P_{CO2}/P_{N2} mixtures were close to the single P_{CO2} and P_{CO2}/P_{N2}. M2 showed a higher P_{CO2}/P_{N2} mixture (64) than M1 (57) at 273 K owing to the difference in CO_2 adsorption capacity, and M2 showed a similar P_{CO2}/P_{N2} mixture (11) than M1 (13) at 448 K.

IV. Conclusion

We successfully synthesized an Al-containing ZSM-58 zeolite membrane on a α-alumina tubular support, which was compared with an all-silica ZSM-58 zeolite membrane. The Al-containing ZSM-58 zeolite membrane could suppress the occurrence of cracks under high-temperature calcination using RTP treatment. The Al-containing ZSM-58 zeolite membrane showed higher separation selectivity than the all-silica ZSM-58 zeolite membrane, and exhibited a CO_2/CH_4 selectivity of 540 and CO_2/N_2 selectivity of 53 at 298 K, and a feed pressure of 0.3 MPa. The ZSM-58 zeolite membrane with high Al concentration is necessary to achieve high separation performance. Although ZSM-58 membrane with Si/Al of 70 could be prepared in this study, the ZSM-58 zeolite crystal can consist of Al to Si/Al of 20. The low Si/Al ZSM-58 zeolite membrane is expected to achieve a high CO_2 separation performance through a surface modification technology such as an amine-modified surface.

Conflict of Interest

The authors declare no conflict of interest.

Author Contributions

Eiji Hayakawa conducted experiment and research under the guidance of Shuji Himeno, and this paper was written jointly Eiji Hayakawa and Shuji Himeno.

Acknowledgment

This work was supported by JSPS KAKENHI Grant (Number 15K12227). The X-Ray fluorescence analysis was performed at the Nagaoka University of Technology Analysis and Instrumentation Center.

References

[1] T. Tomita, K. Nakayama, and H. Sakai, "Gas separation characteristics of DDR type zeolite membrane," *Microporous Mesoporous Mater.*, vol. 68, pp. 71–75, March 2004.

[2] A. Vidoni and D. Ruthven," Diffusion of methane in DD3R zeolite," *Microporous Mesoporous Mater.*, vol. 159, pp. 57–65, September 2012.

[3] L. Bai, C. Liu, M. Li, Y. Wang, G. Nan, D. Hu, Y. Zhang, G. Zeng, W. Wei, and Y. Sun, "Synthesis of all-silica DDR zeolite in an environment-friendly way," *Microporous Mesoporous Mater.*, vol. 239, pp. 34-39, February 2017.
[4] S. Himeno, T. Tomita, K. Suzuki, K. Nakayama, K. Yajima, and S. Yoshida, "Synthesis and permeation properties of a DDR-type zeolite membrane for separation of CO_2/CH_4 gaseous mixtures," *Ind. Eng. Chem. Res.*, vol. 46, pp. 6989-6997, September 2007.
[5] M. Kanezashi, J. O'Brien-Abraham, Y. S. Lin, and K. Suzuki, "Gas permeation through DDR-type zeolite membranes at high temperatures," *AIChE J.*, vol. 54, no. 6, pp. 1478-1486, April 2008.
[6] E. Hayakawa and S. Himeno, "Synthesis of a DDR-type zeolite membrane by using dilute solutions of various alkali metal salts," *Sep. Purif. Technol.*, vol. 218, pp. 89–96, July 2019.
[7] B. Wang, Y. Zheng, J. Zhang, W. Zhang, F. Zhang, W. Xing, and R. Zhou, "Separation of light gas mixtures using zeolite SSZ-13 membranes," *Microporous Mesoporous Mater.*, vol. 275, pp. 191–199, February 2019
[8] Y. Zheng, N. Hu, H. Wang, N. Bu, F. Zhang, and R. Zhou, "Preparation of steam-stable high-silica CHA (SSZ-13) membranes for CO_2/CH_4 and C_2H_4/C_2H_6 separation," *J. Membr. Sci.*, vol. 475, pp. 303–310, February 2015.
[9] S. Li and C. Q. Fan, "High-flux SAPO-34 membrane for CO_2/N_2 separation," *Ind. Eng. Chem. Res.*, vol. 49, pp. 4399-4404, March 2010.
[10] N. Kosinov, C. Auffret, G. J. Borghuis, V. G. P. Sripathi, and E. J. M.Hensen, "Influence of the Si/Al ratio on the separation properties of SSZ-13 zeolite membranes," *J. Membr. Sci.*, vol. 484, pp. 140–145, June 2015.
[11] K. Kidaa, Y. Maetab, and K. Yogo, "Pure silica CHA-type zeolite membranes for dry and humidified CO_2/CH_4 mixtures separation" *Sep. Purif. Technol.*, vol. 197, pp. 116–121, May 2018
[12] M. L. Carreon, S. Li, and M. A. Carreon, "AlPO-18 membranes for CO_2/CH_4 separation," *Chem. Commun.*, vol. 48, pp. 2310-2312, January 2012.
[13] B. Wang, N. Hu, H. Wang, Y. Zheng, and R. Zhou, "Improved AlPO-18 membranes for light gas separations," *J. Mater. Chem. A*, vol. 3, pp. 12205–12212, February 2015
[14] Y. Cui, H. Kita, and K. Okamoto, "Preparation and gas separation performance of zeolite T membrane," *J. Mater. Chem.*, vol. 14, pp. 924-932, January 2004
[15] Structure Commission of the International Zeolite Association. (20 April 2019). Datebase of zeolite structures. [Online]. Available: http://www.iza-structure.org/databases/
[16] L. Wang, C. Zhang, X. Gao, L. Peng, J. Jiang, and X. Gu, "Preparation of defect-free DDR zeolite membranes by eliminating template with ozone at low temperature," *J. Membr. Sci.*, vol. 539, pp. 152–160, October 2017.
[17] M. Wang, L. Bai, M. Li, L. Gao, M. Wang, P. Rao, and Y. Zhang, "Ultrafast synthesis of thin all-silica DDR zeolite membranes by microwave heating," *J. Membr. Sci.*, vol. 572, pp. 567–579, February 2019.
[18] H. G. Karge and J. Weitkamp, "Molecular sieves science and technology," *Springer*, vol. 1, pp. 67–72, 1998.
[19] M. Palomino, A. Corma, F. Rey, and S. Valencia, "New insights on CO_2-methane separation using LTA zeolites with different Si/Al ratios and a first comparison with MOFs," *Langmuir*, vol. 26, no. 3, pp. 1910–1917, February 2010.
[20] N. Kosinov, J. Gascon, F. Kapteijn, and E. J. M. Hensen, "Recent developments in zeolite membranes for gas separation," *J. Membr. Sci.*, vol. 499, pp. 65–79, February 2016.
[21] J. Weitkamp, S. Ernst, T. Bock, A. Kiss, and P. Kleinschmit, "Introduction of noble metals into small pore zeolites via solid state ion exchange," *Stud. Surf. Sci. Catal.*, vol. 94, pp. 278–285, July 1995.
[22] M. Hong, S. Li, H. F. Funke, J. L. Falconer, and R. D. Noble, "Ion-exchanged SAPO-34 membranes for light gas separations," *Microporous Mesoporous Mater.*, vol. 106, pp. 140–146, November 2007
[23] S. R. Venna and M. A. Carreon, "Amino-functionalized SAPO-34 membranes for CO_2/CH_4 and CO_2/N_2 separation," *Langmuir*, vol. 27, pp. 2888–2894, February 2011.
[24] M. Noack, P. Kolsch, A. Dittmar, M. Stohr, G. Georgi, R. Eckelt, and J. Caro, "Effect of crystal intergrowth supporting substances (ISS) on the permeation properties of MFI membranes with enhanced Al-content," *Microporous Mesoporous Mater.*, vol. 97, pp. 88–96, December 2006.
[25] J. Caroa, D. Albrecht, and M. Noack, "Why is it so extremely difficult to prepare shape-selective Al-rich zeolite membranes like LTA and FAU for gas separation?" *Sep. Purif. Technol.*, vol. 66, pp. 143–147, April 2009.
[26] E. Kim, S. Hong, E. Jang, J. H. Lee, J. C. Kim, N. Choi, C. H. Cho, J. Nam, S. K. Kwak, A. C. K. Yip, and J. K. Choi, "An oriented, siliceous deca-dodecasil 3R (DDR) zeolite film for effective carbon capture: Insight into its hydrophobic effect," *J. Mater. Chem. A*, vol. 5, pp. 11246–11254, May 2017.
[27] E. W. Valyocsik, "Crystalline silicate ZSM-58 and process for its preparation using a methyltropinium cation," U.S. Patent 4698217A, Oct. 6, 1987.
[28] Y. Kumita, J. Gascona, E. Stavitski, J. A. Moulijna, and F. Kapteijna, "Shape selective methanol to olefins over highly thermostable DDR catalysts," *Appl. Catal. A: Gen.*, vol. 391, pp. 234–243, January 2011.
[29] S. Heng, P. P. S. Lau, K. L. Yeung, M. Djafer, and J. C. Schrotter, "Low-temperature ozone treatment for organic template removal from zeolite membrane," *J. Membr. Sci.*, vol. 243, pp. 69–78, November 2004.
[30] N. Chang, H. Tang, L. Bai, Y. Zhang, and G. Zeng, "Optimized rapid thermal processing for the template removal of SAPO-34 zeolite membranes," *J. Membr. Sci.*, vol. 552, pp. 13–21, April 2018.
[31] K. S. W. Sing, D. H. Everett, R. A. W. Haul, L. Moscou, R. A. Pierotti, J. Rouquerol, and T. Siemieniewska, "Physical and biophysical chemistry division commission on colloid and surface chemistry including catalysis," *Pure Appl. Chem.*, vol. 57, pp. 603–619, 1985.
[32] J. Kuhn, J. Gascon, J. Gross, and F. Kapteijn, "Detemplation of DDR type zeolites by ozonication," *Microporous Mesoporous Mater.*, vol. 120, pp. 12–18, April2009.
[33] M. A. Ali, B. Brisdon, and W. J. Thomas, "Synthesis, characterization and catalytic activity of ZSM-5 zeolites having variable silicon-to-aluminum ratios," *Appl. Catal. A: Gen.*, vol. 252, pp. 149–162, October 2003.

E. Hayakawa received a BE degree from the Department of Environmental Systems Engineering, Nagaoka University of Technology, Japan, in 2011.

He is currently a graduate student at Nagaoka University of Technology, Japan.